PAPER

Check for updates

Collagen/polyester-polyurethane porous scaffolds for use in meniscal repair†

Gaëlle Savin, [ID] [a,b,d] Sylvain Caillol, [ID] [b] Audrey Bethry,[a] Eric Rondet,[c] Michel Assor,[d] Ghislain David [ID] [b] and Benjamin Nottelet [ID] *[a,e]

Focusing on the regeneration of damaged knee meniscus, we propose a hybrid scaffold made of poly (ester-urethane) (PEU) and collagen that combines suitable mechanical properties with enhanced biological integration. To ensure biocompatibility and degradability, the degradable PEU was prepared from a poly(ε-caprolactone), L-lysine diisocyanate prepolymer (PCL di-NCO) and poly(lactic-*co*-glycolic acid) diol (PLGA). The resulting PEU (M_n = 52 000 g mol^{-1}) was used to prepare porous scaffolds using the solvent casting (SC)/particle leaching (PL) method at an optimized salt/PEU weight ratio of 5 : 1. The morphology, pore size and porosity of the scaffolds were evaluated by SEM showing interconnected pores with a uniform size of around 170 μm. Mechanical properties were found to be close to those of the human meniscus (E_y ~ 0.6 MPa at 37 °C). To enhance the biological properties, incorporation of collagen type 1 (Col) was then performed *via* soaking, injection or forced infiltration. The latter yielded the best results as shown by SEM-EDX and X-ray tomography analyses that confirmed the morphology and highlighted the efficient pore Col-coating with an average of 0.3 wt% Col in the scaffolds. Finally, *in vitro* L929 cell assays confirmed higher cell proliferation and an improved cellular affinity towards the proposed scaffolds compared to culture plates and a gold standard commercial meniscal implant.

1. Introduction

The knee menisci play a crucial role in the knee joint by acting as fibrocartilage discs positioned between the tibia and the femur's condyles. They are vital for bearing and distributing loads, absorbing shocks, stabilizing the joint, and providing lubrication. Unfortunately, as a person ages or experiences joint injuries, meniscal tears frequently happen, and the chances of natural repair are minimal due to the limited ability of articular cartilage to regenerate.[1,2] A limited number of degradable meniscal implants are currently available on the market and used in the clinic. The first one, Collagen Meniscus Implant (Menaflex, formerly called CMI, ReGen Biologics, Franklin Lakes, New Jersey) is composed of 3% of glycosaminoglycan (GAG) and 97% of a type I collagen from

[a]IBMM, Univ Montpellier, CNRS, ENSCM, Montpellier, France.
E-mail: gaelle.savin@enscm.fr, audrey.bethry@umontpellier.fr,
benjamin.nottelet@umontpellier.fr
[b]ICGM, Univ Montpellier, CNRS, ENSCM, Montpellier, France.
E-mail: ghislain.david@enscm.fr, sylvain.caillol@enscm.fr
[c]QualiSud, Univ Montpellier, Avignon Université, CIRAD, Institut Agro, IRD,
Université de la Réunion, Montpellier, France. E-mail: eric.rondet@umontpellier.fr
[d]Arthrocart Biotech, Marseille, France. E-mail: michel.assor@arthrocart.com
[e]Department of Pharmacy, Nîmes University Hospital, 30900 Nimes, France
†Electronic supplementary information (ESI) available. See DOI: https://doi.org/10.1039/d4bm00234b

bovine Achilles tendons. This implant exhibits unwanted folding during surgery due to its poor mechanical properties leading to an uneven pressure, poorer mechanical properties than native menisci.[3–6] On the other hand, the second one, Actifit® (Orteq Ltd, London, United Kingdom), is composed of poly(e-carpolactone)-based polyurethane which leads to appropriate mechanical properties but a very slow degradation (5 years),[7] which may interfere with efficient tissue repair.[8] Tissue engineering for cartilage offers a fresh approach to medical treatment for arthritis, focusing on the repair and regeneration of damaged tissue using cells, growth factors, and a scaffold. The scaffold plays a crucial role in providing support, reinforcement, and organization for the regenerating tissue. The first mission of the scaffold is to replace the damaged meniscus. To achieve this, cell infiltration and proliferation in scaffolds are essential which explains why most scaffolds present a porous structure with uniformly distributed interconnected pores. Among several techniques developed to create such a highly porous structure, solvent casting (SC)/particle leaching (PL) is the most commonly used method. Particles of a specific diameter are incorporated into a polymer solution, then the solvent is evaporated, and particles are leached out by washing in water, leading to a porous structure.[9–11] Different natural polymers have been investigated to replace the meniscus, such as collagen,[12] silk,[13] agarose,[14] hyaluronic acid[15] or alginate.[16] These materials

promote the production of essential compounds like glycosaminoglycans (GAG) that improve extracellular matrix (ECM) deposition. However, they also exhibit weak mechanical strength, uncertain breakdown, and limited availability, limiting their use in regrowing the meniscus. This has led to the widespread use of synthetic materials that offer good strength, predictability, and controlled breakdown for making meniscal scaffolds.[17] Poly(ester-urethane)s (PEUs) are widely used in the biomedical field as they exhibit excellent mechanical and physical properties, tunable degradation rate, and hemocompatibility (no hemolytic activity or activation of thrombus formation) of the scaffold.[18–20] They generally consist of polyester segments linked by urethane bonds obtained by reaction between diol-prepolymers and low molecular weight diisocyanates. The diversity of available polyesters (*e.g.*, PLA, PCL, PLGA) and of diisocyanates (*e.g.*, HDI, LDI), coupled with the possibility to modulate the macromolecular characteristics of the prepolymers (molecular weight, crystallinity, composition) offers an endless array of biomaterials whose mechanical and degradation properties can be matched with the tissue to be engineered.[9–11,21] However, despite their excellent properties, PEUs exhibit low hydrophilicity and lack of physiological activity, which are major limitations for cell adhesion and proliferation.[22]

As a result, to produce an ideal PEU meniscal scaffold, it appears of prime importance to further improve PEU scaffold properties to get closer to the natural environment found in the cartilage matrix. This matrix primarily consists of collagen (type I and type II) and proteoglycans. Collagen is a type of natural polymer (protein) that is widely abundant and possesses highly appealing physiochemical and bioactive properties.[23] Collagen is resorbable and biocompatible with only a minimal immune response since only a small number of people possess humoral immunity against it, making it excellent for cell attachment and biological interactions.[24] Type I collagen (Col-I) is the most common one in the extracellular matrix (ECM), and type II collagen is the primary component of cartilage.[25] It is essential for load transmission between the tibia and femur. Consequently, various natural macromolecules resembling the ECM, such as gelatin or collagen, have been integrated into three-dimensional scaffolds for the purpose of regenerating cartilage.[26–35] Different techniques have been investigated to prepare collagen-functionalized polyurethanes (Col-PUs): covalent immobilization on PU (*e.g.*, by oxygen plasma treatment[36]), collagen-coatings using the electrospinning technique (collagen functionalized PU nanofibers[37]), double-layer-by-layer technology (alternative deposition of positively charged species[22]), or mixing PU with collagen.[32]

In this work, we combine the unique properties of PEU and collagen to develop biodegradable hybrid porous scaffolds suitable for knee meniscus repair. Based on a recent work,[38] we design a PEU obtained from poly(lactic-*co*-glycolic acid) diol (PLGA-diol) and poly(ε-caprolactone)-L-lysine diisocyanate (PCL-LDI) prepolymers (2000 g mol^{-1}) used at an equimolar ratio that serve as segments with high and low glass transition

temperatures (T_g), respectively. The specific composition of the PLGA and the PLGA/PCL ratio are selected to yield more appropriate degradation profiles compared to the whole PCL-based market gold-standard and to maintain suitable mechanical properties for long-term impact reduction in knee meniscus replacement or repair. The process of tissue regeneration with scaffold support is inherently uncertain, influenced by cellular behaviour and their interaction with scaffolds. Consequently, determining the ideal degradation kinetics for a meniscal scaffold is challenging. Nonetheless, it is acknowledged that scaffolds with excessively slow degradation rates may impede effective regeneration and perpetually trigger a foreign body response from the host. On the other hand, LDI is selected to minimize the toxicity associated with the most common diisocyanates and ultimately yield the safe L-lysine after PEU degradation. Porous PEU scaffolds are prepared using the SC/PL technique before homogeneous coating of collagen type I (Col-I) on the surface of pores *via* physical adsorption. It is followed by a thorough characterization of the scaffolds in terms of morphology, porosity, mechanical properties, Col-I repartition and quantification, and degradation kinetics. Finally, we discuss the enhanced biological response of L929 fibroblast cells induced by the Col-I/PEU hybrid scaffolds.

2. Materials and methods

2.1. Reagents and materials

Chemicals. D,L-Lactide (Lot no.: 2009002968) and glycolide (Lot no.: 1210002433) were purchased from Corbion (Gorinchem, The Netherlands). Tin(II) 2-ethylhexanoate (92.5–100%, Lot no.: 1003287404), poly(ε-caprolactone) diol (PCL, M_n = 2000 g mol^{-1}, WXBD4206V), 1,3-propanediol (>98%, Lot no.: S768868143), collagen Type I-fluorescein (col-FITC, Lot no.: SLCM8964), 4-(dimethylamine) benzaldehyde (DMBA, 99%, Lot no.: BCCH7759), sodium acetate anhydrous (>99%), citric acid monohydrate (>98%, Lot no.: SLBL66224V), and chloramine-T hydrate (95%, Lot no.: MKCM5085) were provided by Sigma Aldrich (St-Quentin Fallavier, France) and used as received. 1,4-Dioxane (ACS-Reagent, Lot no.: M1600), distilled in the presence of CaH$_2$, was provided by Honeywell (Offenbach, Germany). Diethyl ether (Batch no.: V1G060031H), acetic acid glacial (Batch no.: 2027/10), sodium hydroxide pellets (Batch no.: V2D06618A) and sodium chloride (Batch number: V1L077212C), were provided by Carlo Erba Reagents (Val de Reuil, France). L-Lysine diisocyanate (LDI; >98%, Lot no.: N04H024) was provided by TCI Europe (Zwikndrecht, Belgium) and used as received. 4-Hydroxy-L-proline (99%, Lot no.: J3514A) was purchased from Alfa Aesar Company (USA). Type I acid soluble collagen (Lot no.: 20ACI060) was purchased from Symatese (Chaponost, France). Deuterated chloroform (Lot no.: T2811) was purchased from Eurisotop (St-Aubin, France). Iohexol was provided by Thermo Fisher Scientific (Illkirch, France).

For biological assays. 0.1% zinc diethyldithiocarbamate polyurethane film (ZDEC, Lot no.: A-223K) and high-density

polyethylene film (Lot no.: C-221) were provided by Hatano Research Institute, Food and Drug Safety Center (Japan). Dulbecco's modified Eagle's medium (DMEM/F-12, Lot no.: RNBL4062), (Lot no.: 0000205667), Human/Murine/Rat BMP-2 (Lot no.: 0719255 BO123), and GlutaMAX™ (Lot no.: 2554717) were purchased from Thermo Fisher (Massachusetts, USA). Tissue Culture Polystyrene (TCPS) 96-well plates and 48-well plates were purchased from Becton Dickinson (Le Pont-de-Claix, France). Phalloidin-iFluor 488 was provided by Abcam (Cambridge, United Kingdom). PrestoBlue™ HS cell viability reagent (Lot no.: 2615830) was provided by Invitrogen (Oregon, USA). CellTiter-Glo® Luminescent Cell Viability assay (Lot no.: 0000497159) was provided by Promega (Charbonnières-les-Bains, France). Hoechst 33342 solution (Lot no.: 404P189) was purchased from PromoKine (Heidelerg, Germany).

Actifit® scaffold used as the gold standard control material was kindly provided by MD. Michel Assor from Vert Coteau Hospital (Marseille, France).

2.2. Nuclear magnetic resonance (NMR)

All ^{1}H NMR analyses were done on a Bruker Avance III HD 400 MHz NMR equipped with a BroadBand Inverse (BBI) probe. ^{1}H and 2D NMR spectra were recorded at 298 K on a Bruker Avance III 600 MHz NMR spectrometer using a TCI Cryoprobe Prodigy®. 2D homonuclear ^{1}H–^{1}H g-COSY (1 scan, 256 real (t1) × 2048 (t2) complex data points) and 2D heteronuclear spectra ^{13}C–^{1}H g-edited HSQC (2 scans, 256 real (t1) × 2048 (t2) complex data points) were recorded to assign the compound. All Chemical shift data are given in δ ppm calibrated with a residual protic solvent (*e.g.* CDCl$_3$: 7.26 ppm – [1]H/77.16 ppm – [13]C). Spectra were processed and visualized with Topspin 3.6.2 (Bruker Biospin) on a Linux station.

2.3. Fourier transform infrared (FTIR) spectroscopy

Infrared spectra of the polymers were collected using a Fourier transform infrared (FTIR) spectrophotometer. Measurements were carried out using attenuated total reflection (ATR) in transmission mode with a Thermo Fisher Scientific (Waltham, MA, USA) Nicolet iS50 FT-IR Flex Gold spectrometer equipped with a deuterated triglycine sulfate (DTGS) detector. The characteristic IR absorption bands are reported in cm^{-1}. Each sample was scanned 32 times at a resolution of 4 cm^{-1} over the frequency range of 4000–400 cm^{-1}.

2.4. Isocyanate equivalent weight (IEW) and hydroxyl equivalent weight (HEW)

The IEW of LDI and PCL-LDI prepolymer, and the HEW of PCL-diol and PLGA-diol, were determined by ^{1}H NMR titration, using benzophenone as the internal standard. For each compound, three samples were prepared with approximately 20 mg

of benzophenone and 50 mg of the sample dissolved in 0.5 mL of CDCl$_3$ and analysed by ^{1}H NMR. The IEW and HEW were determined by integration of the signals at 3.3 and 4.0 ppm for LDI; 4.3 ppm and 4.20 ppm for PLGA; 3.6 ppm for PCL and 7.5 ppm for benzophenone. An example is given for the IEW calculation of LDI, in eqn (1), where $N_{\text{H eq LDI}}$ corresponds to the average number of hydrogens in alpha to the isocyanate moiety (2H at 3.3 ppm and 1H at 4 ppm).

$$\text{IEW(LDI)} = \frac{m_{\text{LDI}} \times N_{\text{H eq LDI}} \times \int_{7.28}^{7.87} \text{benzophenone}}{m_{\text{benzophenone}} \times N_{\text{N eq benzophenone}} \times \left(\int_{3.28}^{3.34} \text{LDI} + \int_{4.00}^{4.04} \text{LDI} \right)}. \tag{1}$$

The IEW of the prepolymer was determined by ^{1}H NMR titration (IEW = 1053 g per eq.).

The IEW and HEW of the precursors of interest are summarized in Table S1.†

2.5. Thermogravimetric analyses (TGA)

Thermogravimetric analyses (TGA) of PEU were performed on a NETZSCH TG 209 F1 Libra® (Selb, Germany) TGA under 50 mL min^{-1} argon. The protective gas used was argon with a 20 mL min^{-1} flow. Approximately 10 mg of the sample was placed in an alumina crucible and heated from room temperature to 800 °C with a 20 °C min^{-1} heating ramp to allow rapid estimation of the thermal stability of our samples.

2.6. Differential scanning calorimetry (DSC)

Differential scanning calorimetry (DSC) measurements were performed using a NETZSCH DSC 3500 Sirius (Selb, Germany). Constant calibration was performed using indium, *n*-octadecane, *n*-octane, adamantane, biphenyl, tin, bismuth and zinc standard. Nitrogen was used as the purge gas at 40 mL min^{-1}. Approximately 10 mg of sample was placed in pierced aluminium pans and the thermal properties were recorded between −150 °C and 200 °C at 20 °C min^{-1} to observe the glass transition temperature (T_g). Glass transition temperatures were measured on the second heating ramp to erase the thermal history of the polymer.

2.7. Size exclusion chromatography multi-angle light scattering (SEC-MALS)

SEC-MALS measurements were performed on an Agilent 1260 Infinity triple detection SEC set-up (Santa Clara, CA, USA) comprising a Wyatt Optilab MALS detector, and an Agilent differential refractometer. Separation was achieved using 2 PLgel mixed B LS columns (7.5 mm × 300 mm). The eluent was tetrahydrofuran (THF) at 30 °C at a flow rate of 1 mL min^{-1}. The refractive index increment (dn/dc) of PLGA, PCL, the prepolymer and PU was obtained as follows. Five different concentrations (0.25 mg mL^{-1}, 0.5 mg mL^{-1}, 0.75 mg mL^{-1}, 1 mg mL^{-1}, 1.5 mg mL^{-1}, and 2 mg mL^{-1}) of the polymer in THF were injected and the resulting RI signals were plotted as a function of concentration. The dn/dc values of the polymers

are given in Table S2† and were used for the MALS analysis of all samples in this work.

2.8. Scanning electron microscopy (SEM)

The scaffolds were evaluated using a scanning electron microscope Phenom ProX Desktop from Thermo Fisher Scientific (Waltham, MA, USA). The scaffolds were freeze-dried prior to analysis. For each sample, 3 different sections of 2 mm were fixed to a sample holder, with a conductive carbon ribbon.

The sections were then sputter coated with gold (thickness of 10 nm) to analyse the porous structure at 10 kV. Pore size distribution and average pore size in the samples were characterized with the ImageJ program. Pore sizes are expressed as mean ± SD ($n = 80$).

2.9. Mechanical properties

Cubic samples (10 mm per side) were cut for testing. Compressive strengths at 20% deformation and Young's modulus were determined using an Instron® tester model 3366 (Norwood, MA, USA) equipped with a 100 N load cell. The measurements were carried out at a crosshead speed of 5 mm min^{-1}. All given values are given as means of three measurements ± SD. The modulus was determined from the slope of the linear portion of the stress–strain at a compressive strain of 20%.

The same experiment was conducted on wet samples. Cubic samples were immersed in water at 37 °C under stirring (100 rpm) for 24 h. A BioPuls Bath accessory with water at 37 °C was installed on the machine, and the compression modulus was measured. To avoid slippage during the wet experiments, the upper part was placed in contact with the material, while applying a preload of 0.01 N, which had no impact on the maximum load of 2 N of the sample.

2.10. Dynamic mechanical analyses (DMAs)

Dynamic Mechanical Analyses (DMAs) were carried out on a Mettler Toledo DMA instrument with STARe software. Cubic specimens (5 × 5 × 5 mm) were used. The thickness of the sample was measured with a caliper. Compression of samples was performed while heating at a rate of 2 °C min^{-1} from 15 °C to 60 °C, keeping the frequency at 1 Hz. The loss modulus (E'') and storage modulus (E') were expressed in MPa, and tan(δ) was dimensionless, as seen in eqn (2). T_α was obtained at the maximum value of tan(δ).

$$\tan(\delta) = \frac{E''}{E'}. \qquad (2)$$

2.11. Poly(ester-urethane) synthesis

The synthesis of the PLGA-diol and of the PCL-diol have been described previously and were identical in the present work.[38] PLGA with an equimolar ratio of lactide and glycolide was synthesized to ensure suitable degradability. The synthesis of the prepolymer PCL-LDI was conducted as follows: 10.2 g of LDI (IEW = 116 g per eq., 2.5 eq.) was introduced into a dried 250 mL, two-neck, round-bottom flask. The system was purged

with 3 cycles: nitrogen/vacuum, and then heated up to 80 °C. 39.82 g of PCL (HEW = 1135 g per eq.) was solubilized in 60 mL of toluene and added dropwise with a syringe driver for one hour (60 mL h^{-1}) with magnetic stirring. The mixture was stirred for an additional 3 h. Then, the prepolymer was precipitated in 800 mL of cold pentane. The prepolymer was collected by filtration and dried at 40 °C under vacuum for 24 h. It was stored at −20 °C. The chemical shifts and integrations of the different signals of the PEU NMR spectrum are given in the following paragraph.

^{1}H-NMR (400 MHz, CDCl$_3$, ppm) δ = 4.26 (q, 1.76H, H$_w$), δ = 4.2 (m, 2.9H, H$_{w'}$), δ = 4.1 (m, 4H, H$_i$), 4.0 (m, 35H, H$_h$), 3.98 (m, 1H, H$_v$), 3.3 (m, 1.2H, H$_{v'}$), 3.1 (m, 3.5H, H$_m$), 2.3 (t, 38H, H$_n$), 1.7 (m, 4H, H$_j$), 1.6 (m, 84H, H$_p$), 1.5 (m, 4H, H$_j$), 1.3 (m, 40H, H$_r$) 1.2 (m, 2H, H$_s$) (Fig. S1†).

The extension of the PCL-LDI prepolymer with PLGA was previously described,[38] and the same method was used with prepolymer functionalized with LDI. Briefly, 7 g of PLGA (HEW = 1120 g per eq.) was added into a dry glass reactor purged with nitrogen, with 10 mL of distilled dioxane. The reactor was heated to 100 °C, and 8 g of PCL-LDI prepolymer (IEW = 1053 g per eq.) was added, with tin(II) 2-ethylhexanoate (0.5 wt%). The system was reacted with a mechanical stirring blade at this temperature for 1 h, until the disappearance of isocyanate band at 2300 cm^{-1}. Following the polyaddition, distilled dioxane was slowly added to control the viscosity of the mixture and allow the transfer and use of the PEU. The polymer was purified by precipitation in 80 : 20 diethylether : EtOH, with a final yield of 84%.

2.12. Scaffold preparation

Porous polymer scaffolds were prepared by SC/PL with NaCl salt as the porogen agent. Briefly, 3 g of PEU was dissolved in 9 mL of THF and 15 g of NaCl crystals (sieved to 100–300 µm) were added to the polymer solution. After vigorous mixing, the suspension was poured into a mould, and rapidly frozen by immersion into liquid nitrogen before evaporation of the solvent at room temperature overnight. The scaffold was washed in distilled water at room temperature, for 3 days, until clearance of salt crystals.

To characterize the scaffold, the porosity was calculated according to eqn (3), where m is the mass of the scaffold (g), V is the volume of the scaffold (cm^3), and ρ_{PEU} is the volumic mass of the PEU (1.07 g cm^{-3}). Porosity values are the mean of three measurements ± SD.

$$P = \left(1 - \frac{m}{\rho_{PEU}V}\right) \times 100. \qquad (3)$$

2.13. Collagen incorporation

Different techniques were tested to incorporate the collagen within the scaffold: soaking, injection and forced infiltration with different collagen concentrations.

Soaking. Scaffolds were placed in the Col-I solution for 24 h and lyophilized.

Injection. The Col-I solution was injected within the scaffold at different locations with a syringe.

Forced infiltration. Scaffolds (9 mm diameter) were introduced in a 5 mL syringe filled with Col-I solution at a concentration of 3 mg mL^{-1}. Pressure was applied to release the collagen solution out of the syringe. The scaffold was left at room temperature to evaporate the acetic acid. After 3 injections, the PEU scaffold coated with Col-I (PEU-Col) was freeze-dried.

2.14. Determination of collagen content by SEM-energy dispersive X-Ray (SEM-EDX) analysis

EDX was employed to detect the augmentation of nitrogen atoms on the samples after collagen treatment. 3 sections of 2 mm for each sample were fixed to a sample holder with a conductive carbon ribbon.

Maps of the relative distribution of carbon, oxygen and nitrogen were acquired at 10 kV. Average nitrogen weight percentages are expressed as mean ± SD (3 maps for each section). SEM-EDX was also performed on a collagen film to evaluate the nitrogen weight percentage: N wt% = 23.8 ± 4.5%.

Collagen content was then calculated using eqn (4).

$$\text{Collagen content(wt \%)} = \frac{\text{Nitrogen of collagen within the scaffold(wt\%)}}{\text{Nitrogen of a collagen film(wt\%)}}. \quad (4)$$

2.15. Determination of collagen content from hydroxyproline content

The collagen content within the scaffold was determined from the hydroxyproline content.[39] Briefly, the scaffold coated with collagen was immersed in acetic acid to release collagen. After evaporation, the collagen was hydrolysed in HCl 6 N at 100 °C overnight. HCl was then evaporated and the collagen was dried under vacuum for 5 hours. The resulting dried collagen was dissolved in distilled water.

Hydroxyproline solutions were prepared at different concentrations to obtain the calibration curve. The solutions and collagen were then reacted with chloramine-T for 20 min at RT. Excess chloramine-T was decomposed by the addition of perchloric acid at 3.15 M. After 5 min, dimethylaminobenzaldehyde was added and the samples were placed in an oven at 60 °C. After 20 min, the samples were cooled for 5 min at 4 °C. The absorbance was measured at 557 nm using a PerkinElmer UV/VIS Lambda 360 spectrometer. The hydroxyproline value was determined directly from the calibration curve.

2.16. Determination of collagen content from COL-FITC

The collagen content was also determined from the fluorescence of Col-FITC. The scaffold was subjected to the same coating, as explained in section 2.12, with Col-FITC. The scaffold was immersed for 24 h in acetic acid to release the collagen content. The fluorescence of this solution was measured with a spectrofluorophotometer Shimadzu RF-5301PC (Noisiel, France) at a wavelength of 491 nm, an excitation width of 20 nm, and an emission width of 5 nm. The fluorescence of the solution could be linked to the collagen content thanks to the calibration curve, obtained with the fluorescence of different Col-FITC solutions, at known Col-FITC concentrations.

2.17. Micro-computed tomography

Image acquisition. Samples with 8 mm diameter, and 1 mm thickness were placed in a SkyScan 1272 X-ray microtomograph (Bruker μCT, Kontich, Belgium) without a filter at a pixel size of 3 μm with an applied X-ray tube voltage of 38 kV and a source current of 242 μA. A camera pixel binning of 4032 × 2688 was applied. The scan orbit was 180° with a rotation step of 0.2°.

Two scaffolds were analysed to visualize the morphology of the scaffolds and quantify collagen content. To visualize the collagen coating, 1 g of iohexol was solubilized in 17 mL of collagen solution prior to coating according to the procedure described in section 2.13.

Image reconstruction. Reconstruction was carried out with a modified Feldkamp algorithm,[40] using the SkyScan™ NRecon software accelerated by GPU.[41] Gaussian smoothing, ring artefact reduction and beam hardening correction were applied.

Image analysis. Volume of interest selections (sample volume), segmentations to binary and morphometric analysis of the samples were all performed using SkyScan CT-Analyser ("CTAn") software. Image segmentation to binary was carried out thanks to a global segmentation algorithm. Morphometric parameters in 3D (porosity, pores size) were based on the analysis of a Marching Cubes[42] type model with a rendered surface. The pore size in 3D was calculated using the local thickness or "sphere-fitting" (double distance transform) method.[43,44] Note that for the porosity, this analysis makes it possible to distinguish between closed porosity and open porosity. In contrast to open porosity, closed porosity is the porosity embedded in the polymer with no contact with the environment.

2.18. Sterilization

Gamma-ray sterilization of the PEU scaffolds was performed to evaluate its impact on the scaffolds' mechanical properties. The sterilization procedure was performed using Ionisos (Chaumesnil, France) with the following parameters: frequency 640 Hz, scan width 2.6 A, one turn at 0.6 m min^{-1}. The sample was exposed at a controlled speed to gamma radiation (25 kGy ± 10%) for 9.5 hours, generated from an electron beam machine.

2.19. Cytotoxicity study

The cytotoxicity of the scaffolds was investigated through the quantification of adenosine triphosphate (ATP) using a SpectraMax® i3x plate reader (Molecular Devices). Cells and control polymers were chosen in accordance with NF EN ISO-10993 guidelines.

L929 murine fibroblasts. The cytotoxicity of the PEU film was investigated on a murine fibroblast cell line, L929

(NCTC-Clone 929, ECACC 85011425). L929 cells were cultured at 37 °C under humidified 5% CO_2 in Dulbecco's Modified Eagle's medium 4.5 g L^{-1} D-glucose supplemented with 2 mM L-glutamine, 5% v/v fetal bovine serum, and 100 U mL^{-1} penicillin and 100 μg mL^{-1} streptomycin.

CellTiter-Glo® Luminescent Cell Viability assay (*Promega G7571, Lot No.: 0000497159*): a PU film containing 0.1% ZDEC, batch A-223K, was used as the positive reference material (RM-A) and HDPE, batch C-221, was used as the negative reference material (RM-C). The PEU film, positive and negative RMs were irradiated at λ = 254 nm for 2 minutes, twice on each face for decontamination. Specimens were placed in the culture medium (100 mg mL^{-1}) and incubated for 72 h at 37 °C under stirring. The cells were seeded into a 96-well plate at a density of 6×10^4 cells per well and incubated overnight at 37 °C under humidified 5% CO_2. Then, the medium in contact with the materials was extracted and 100 μL was incubated with the cell monolayer for an additional 24 h. The number of viable cells was obtained by a CellTiter-Glo® assay, based on the quantification of the present ATP, which represents metabolically active cells. The CellTiter-Glo® reagent was added to each well and the plate was placed at room temperature for 10 minutes to stabilize the luminescent signal before reading. The background, corresponding to wells free of cells, was subtracted from each triplicate mean.

2.20. Cell proliferation assessment (PrestoBlue™ Assay)

L929 fibroblasts were seeded in 48-well plates at a concentration of 30 000 cells per well (70 μL added) using the serum-based medium. At determined time points (twice a week), the medium was refreshed, and cells were incubated with 10% PrestoBlue™ (Lot no.: 2615830) at 37 °C with 5% CO_2 for 40 min. A sample of 200 μL of PrestoBlue™ solution was then transferred into a black 96-well plate for fluorescence reading at 560 nm and 590 nm using a plate reader (Spectramax i3x, Molecular Devices). The proliferation of fibroblasts was determined by the increase in PrestoBlue™ reduction at 2, 4, 9 and 14 days. Data are expressed as means ± SD and correspond to measurements with n = 6 for TCPS, PEU and PEU-Col scaffolds, and n = 4 for the gold standard due to the low availability of this product at the stage of the performed experiments.

2.21. Visualization of cells on the scaffolds

Cells on scaffolds were observed using actin filaments and nucleus staining. At the end of the proliferation study (14 days), scaffolds were rinsed 2 times with PBS. Then, they were fixed with paraformaldehyde 4% for 30 min at room temperature. The cells were permeabilized with Triton X100 for 20 min. After 3 washes in PBS, cell actin filaments and nuclei were stained with phalloidin-iFluor 488 (Green) and Hoechst (Blue) for 45 min in the dark and room temperature. The scaffolds were then rinsed 3 times with PBS and the cells were examined with a Leica Thunder microscope with 460 nm and 488 nm filters. The obtained fluorescence image results were analysed using FIJI software.

2.22. Degradation study

The kinetics of degradation was studied *in vitro* under standard conditions according to ISO-13781:2017, using phosphate buffer solution (PBS, pH = 7.4) at constant temperature (37 °C) and under continuous stirring (100 rpm). Scaffold samples were cut into a cubic shape, weighed ($w_{dry, t0}$) and incubated in 1 mL of PBS solution (pH = 7.4). The samples were removed from the medium at specific time points, washed with distilled water, carefully wiped and then dried to a constant weight ($w_{dry,t}$). The solution was replaced when pH decreased of 5%. Degradation was monitored by determination of the weight loss, molecular weight of the PEU and Young's modulus. The remaining weight was calculated from eqn (5) and the remaining molecular weight from eqn (6), and the remaining Young's modulus from eqn (7). M_{n0} is the initial molecular weight an M_{nt} the molecular weight after t time in PBS. E_{y0} is the initial Young's modulus and E_{yt} is the Young's modulus after t time in PBS.

$$\text{Remaining mass}(t)(\%) = \left(1 - \frac{w_{dry,t0} - w_{dry,t}}{w_{dry,t0}}\right) \times 100 \quad (5)$$

$$\text{Remaining } M_n(t)(\%) = \left(1 - \frac{M_{n0} - M_{nt}}{M_{n0}}\right) \times 100 \quad (6)$$

$$\text{Remaining } E_y(t)(\%) = \left(1 - \frac{E_{y0} - E_{yt}}{E_{y0}}\right) \times 100. \quad (7)$$

2.23. Statistical analysis

All results are presented as means ± standard deviations. The proliferation data were analysed using the Kruskal–Wallis test followed by a Dunn *post-hoc* test to determine significant differences between groups (R software version 3.6.1). A confidence interval of 95% was used and differences were considered significant when $p < 0.05$.

3. Results and discussion

3.1. Poly(ester-urethane) synthesis

PCL-diol with a molar mass of 2300 g mol^{-1} according to the ^{1}H NMR calculation was end-capped with an excess of LDI at 80 °C to obtain the prepolymer (see Fig. S1†). Bruin *et al.*[45] reported the synthesis of biodegradable PEU using LDI, which did not produce adverse tissue reactions. Moreover, other researchers used LDI and proved that no significant toxic or tumorigenic responses to the materials were found.[46]

The derivatization of PCL-diol towards PCL-LDI was monitored by ^{1}H NMR spectroscopy. Different protons were assigned by COSY and HSQC analyses, as seen in Fig. S1 and S2,† respectively. Spectra showed the complete disappearance of the signal from the CH_2 close to the hydroxyl groups of PCL-diol at 3.7 ppm and the appearance of new signals at 3.10 (H_d) and 3.3 ppm ($H_{a'}$) corresponding respectively to the methylene in the α-position of the urethane function, and the methylene in the α-position of the isocyanate function. LDI has two iso-

cyanate moieties in α and ε positions with different reactivities. In fact, the isocyanate group in the α-position is expected to exhibit lower reactivity than the one in the ε-position due to its secondary nature. To analyse the reactivity of the different isocyanate groups, the intensity of the integrations of Hv′ and Hm was used. $H_{v′}$ is representative of urethane formed from the reaction of secondary isocyanates (left part on the prepolymer structure in Fig. S1†), whereas H_m corresponds to the hydrogen next to the urethane group from the reaction of primary isocyanate (see the right part in Fig. S1†). By calculating the ratio of these two integrations, we can conclude that 75% of the prepolymer chains are end-capped with a primary isocyanate, and 25% by a secondary isocyanate.

The synthesis of the PCL-LDI prepolymer was further confirmed by FTIR spectroscopy, with spectra showing a sharp peak at 2300 cm^{-1} corresponding to the stretching vibration of the isocyanate group N=C=O.

The isocyanate terminated prepolymer was then extended with PLGA-diol with the 1.1 : 1 ratio to yield the targeted PEU. A typical PEU ^{1}H NMR spectrum is displayed in Fig. 1A, which confirmed the equimolar composition in PCL and PLGA segments in the PEU structure. The molecular weight of PEU was determined by SEC-MALs analyses with M_n = 52 kg mol^{-1}, M_w = 100 kg mol^{-1}, and Đ = 1.8 (Fig. 1B). This high molecular weight should ensure good mechanical properties of the scaffolds thanks to the expected high degree of entanglement and to the hydrogen bonds between urethane groups. The thermal properties of PEU were investigated (as shown in Fig. 1C for DSC thermograms, and in Fig. S3† for TGA), and were similar to the PEU formed with HDI as building blocks with T_m at 50 °C and T_g at −50 °C.[38]

3.2. Scaffold preparation

A scaffold designed to effectively repair the meniscus should possess several key features. It should have large pores to facilitate cell ingrowth, exhibit favourable mechanical properties, and possess high porosity. The parameters to yield a scaffold using the salt and leaching process were selected based on our previous work. However, to ensure smooth solvent evaporation, THF with a low boiling point (T_{eb} = 66 °C), was chosen instead of dioxane. Salt particles were mixed with the PEU solution in THF at the previously optimized concentration (5 g of salt per g of PEU) to ensure good balance between porosity and mechanical properties. This suspension was then left to evaporate at room temperature to yield the scaffold that was then immersed in water to remove the salt crystals before final
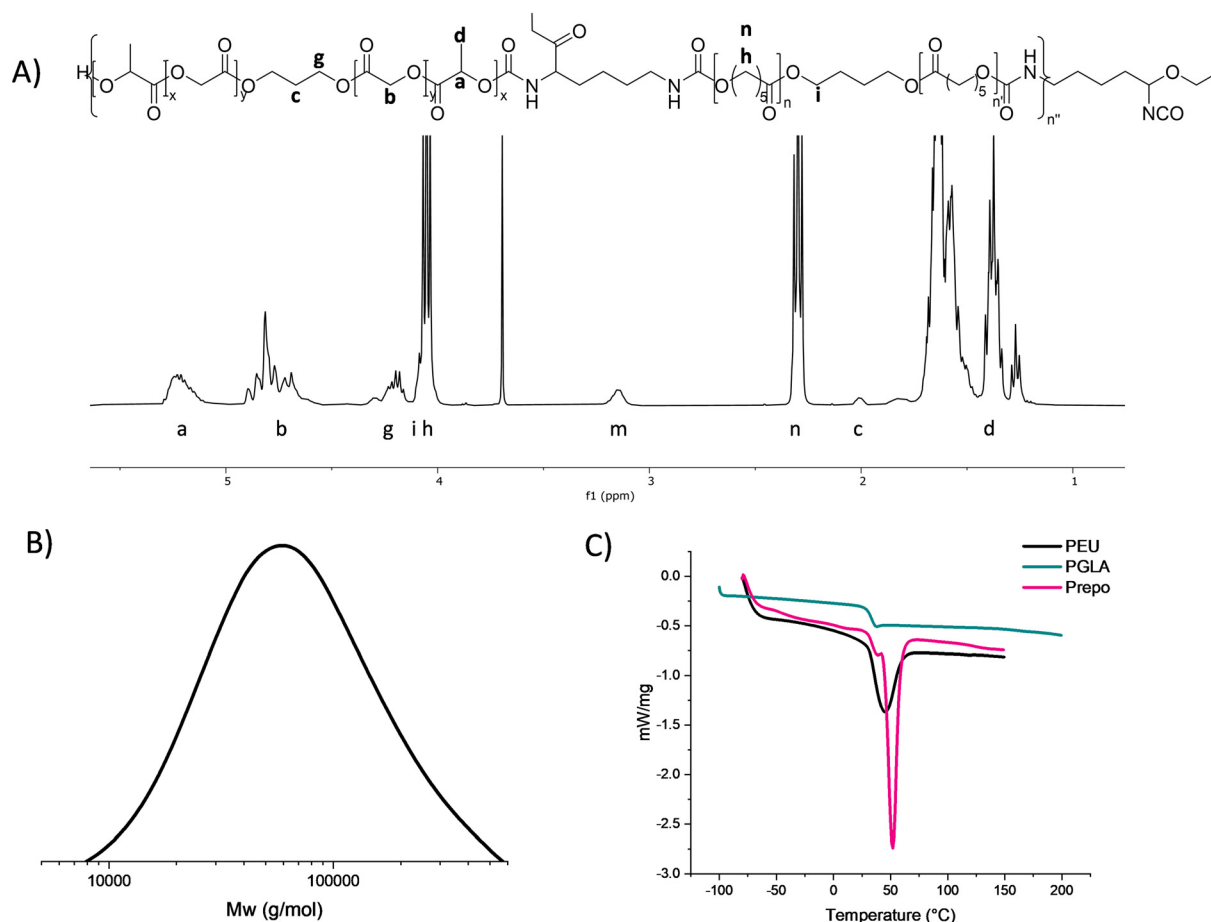

Fig. 1 Physicochemical characterization of the PEU. (A) ^{1}H NMR in CDCl$_3$, (B) chromatogram of PEU (SEC–MALS THF), and (C) DSC thermograms.
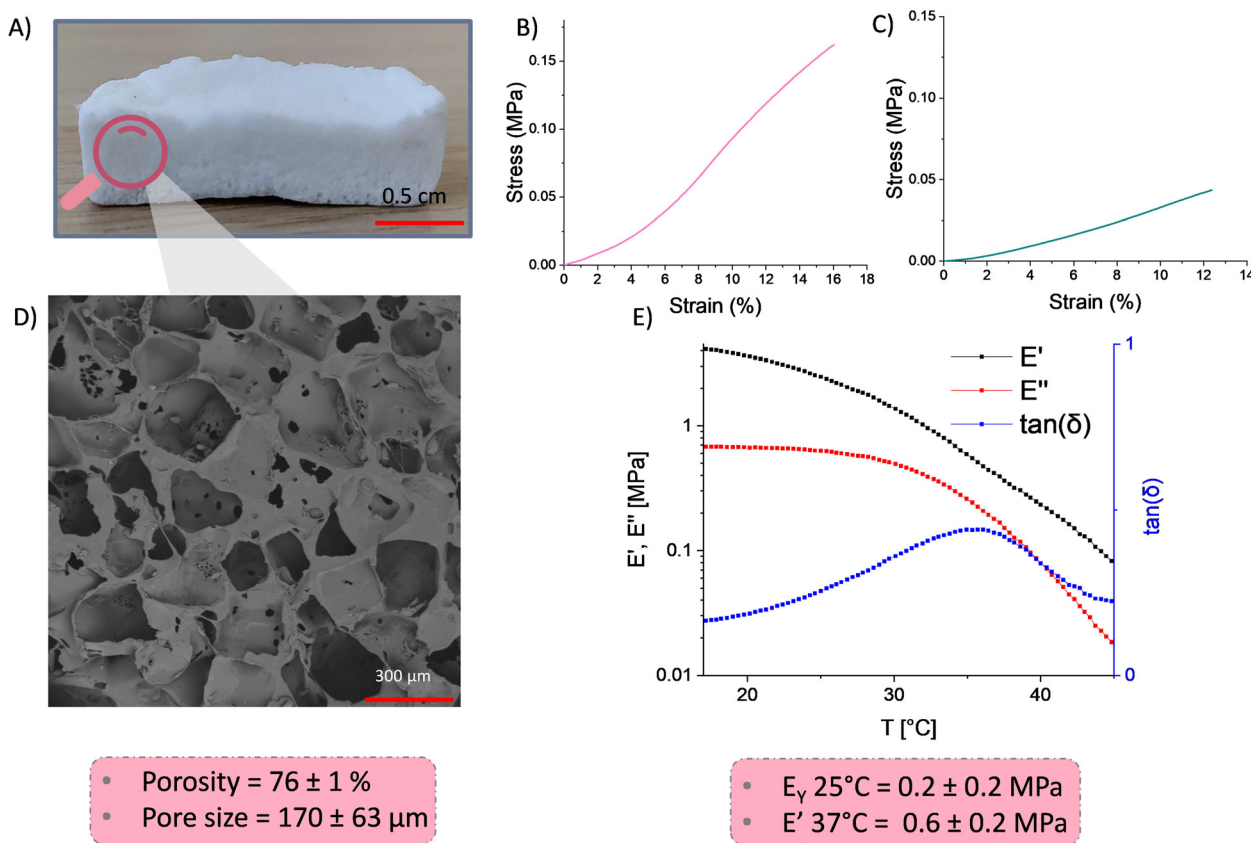
Fig. 2 Morphological and mechanical characterization of the PEU scaffold. (A) Macroscopic picture of a PEU scaffold, (B) typical stress/strain compression curve under dry conditions at RT, (C) typical stress/strain compression curve of PEU scaffold immersed in water at 37 °C, (D) SEM micrograph of the inner part of a PEU scaffold, and (E) thermo-mechanical analyses of PEU scaffolds analysed by DMA (storage modulus E', loss modulus E'' and loss factor tan(δ)).

freeze-drying. The resulting scaffolds were obtained in the form of white scaffolds (Fig. 2A). By analysing the SEM images, an average pore size of 170 ± 63 μm, corresponding to the size of the added NaCl crystals (150–300 μm), was calculated (see Fig. 2D and Fig. S4†). The porosity of the scaffold, determined by the volumic mass ratios of the PEU and scaffold (see eqn (3)), was 76 ± 1%, which is sufficient to guarantee cell proliferation. After conducting these morphological analyses, the mechanical properties of the scaffolds were investigated. In a typical stress/strain curve, (Fig. 2B), the Young's modulus E_y at 25 °C was 0.2 ± 0.2 MPa, in accordance with the mechanical properties of the human meniscus (E_y = 0.6 MPa).[47] This value is comparable to that of scaffolds previously obtained with HDI (Ey = 1 ± 0.1 MPa), with a similar porosity of 74% (see Fig. S5†). Furthermore, to mimic physiological conditions, mechanical properties were measured on wet samples in a bath at 37 °C (see Fig. 2C). The Young's modulus was 0.18 ± 0.03 MPa, which is, as expected, lower compared to dry samples. Dynamic analyses were carried out to confirm the results obtained from static analyses: storage modulus at 25 °C was 3.8 ± 0.7 MPa, and at 37 °C: 0.6 ± 0.2 MPa (Fig. 2E): T_α of the scaffold was 36 ± 0.1 °C, close to the glass transition of PLGA blocks.

3.3. Collagen incorporation

To enhance the biological properties of the scaffold, collagen incorporation was then performed. Different techniques were tested to incorporate collagen within the scaffold: soaking, injection and force infiltration at different collagen concentrations (see Fig. 3A). We first investigated the influence of the collagen concentration on the extent of collagen content in the final scaffold by soaking. The weight percentage of nitrogen was higher (9.2 ± 2.3%) after 24 h soaking into a collagen solution at 3 mg mL^{-1} compared to 1 mg mL^{-1} (7.8 ± 3%) and 5 mg mL^{-1} (6.7 ± 1.5%). Indeed, the viscosity of the collagen solution at 5 mg mL^{-1} was too high to easily penetrate the pores. Following this first assay, the collagen concentration of 3 mg mL^{-1} was selected to test the other two incorporation techniques: injection and forced infiltration. The injection method gave the lowest percentage: 4.1 ± 0.4 wt%. In the last method, three successive forced infiltrations were performed. Fig. 3B and C show the overall repartition of oxygen, carbon and nitrogen atoms in the scaffolds before and after collagen incorporation by forced infiltration, whereas Fig. 3E and F focus only on nitrogen atoms. These analyses confirm that the nitrogen density is higher in the PEU-Col scaffold, and that
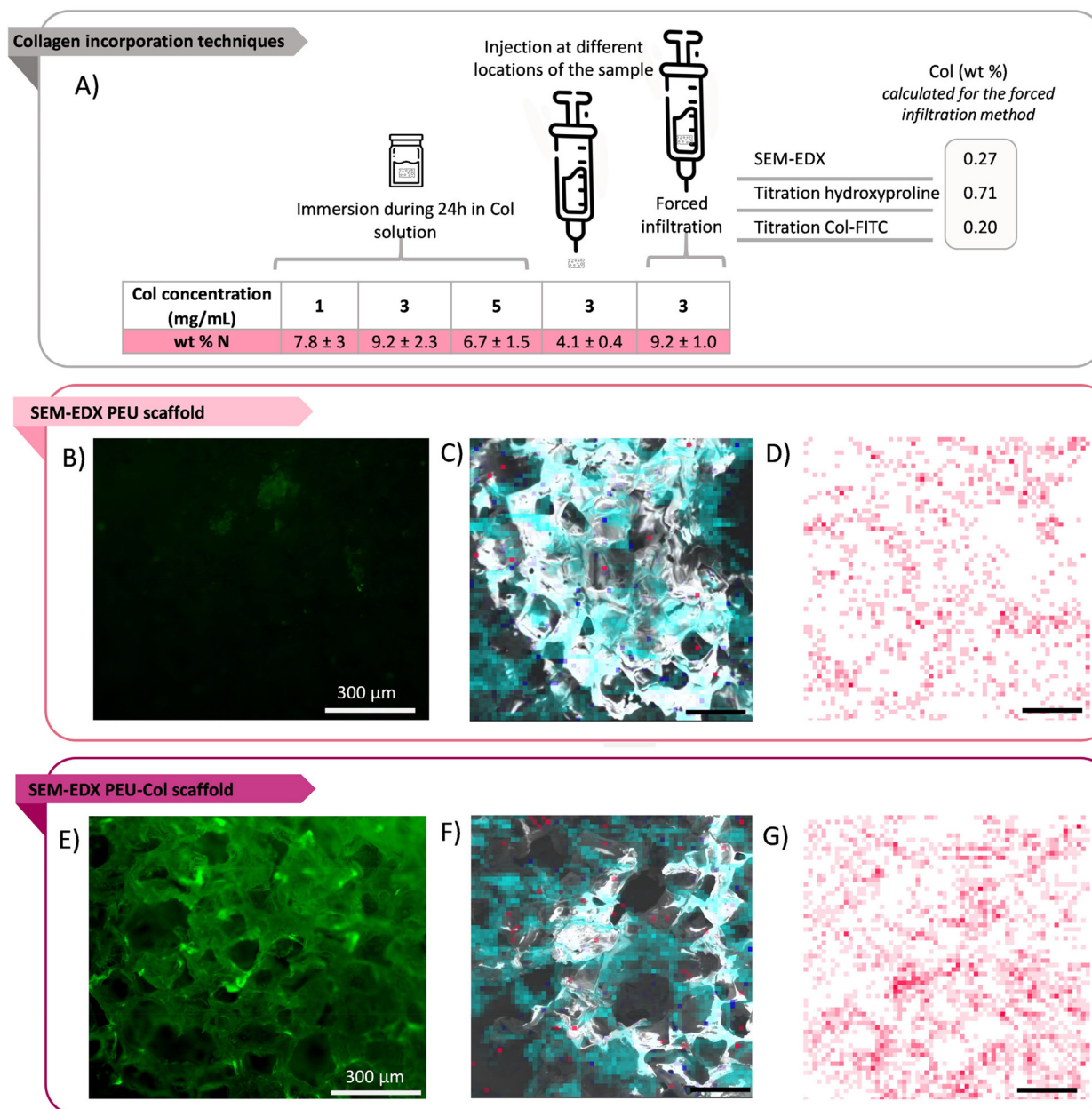
Fig. 3 Evaluation of the collagen incorporation in the PEU scaffolds. (A) Comparison of the weight percentage of nitrogen in scaffolds as a function of the method used for the incorporation and comparison of the weight percentage of collagen in the scaffold as a function of different characterization techniques; (B & E) fluorescence micrograph of the scaffold before/after Col-FITC coating respectively; (C & F) SEM-EDX of the scaffold before/after collagen coating respectively; (D & G) SEM-EDX with nitrogen atoms only of the scaffold before/after collagen coating respectively. Scale bar corresponds to 300 µm. Data are expressed as means $\pm$ SD and correspond to measurement with $n = 3$.

collagen is homogeneously spread in all pores. This was further confirmed by the visualization of a Col-FITC coating, as seen in Fig. 3D. The fluorescence imaging clearly proves this homogeneous coating of pores by the collagen.

In the next step, to quantitatively evaluate the nitrogen content increase, the integration of the nitrogen signal in the EDX spectra was calculated (see Fig. 4).

The weight percentage of nitrogen showed a 6.6 wt% increase in the N content after forced infiltration. SEM-EDX

was also performed on a collagen film to evaluate the nitrogen weight percentage that corresponds to 23.8 $\pm$ 4.5 wt%. This allowed us to estimate a collagen content of 0.3 wt% in the scaffold by EDX. Overall, forced infiltration was selected as the more efficient, fast and convenient method to coat the PEU scaffolds with Col-I.

To confirm this value of 0.3 wt% collagen in the scaffolds, the collagen content was further determined by calculating the absorbance value of hydroxyproline (Table S3†) present in a
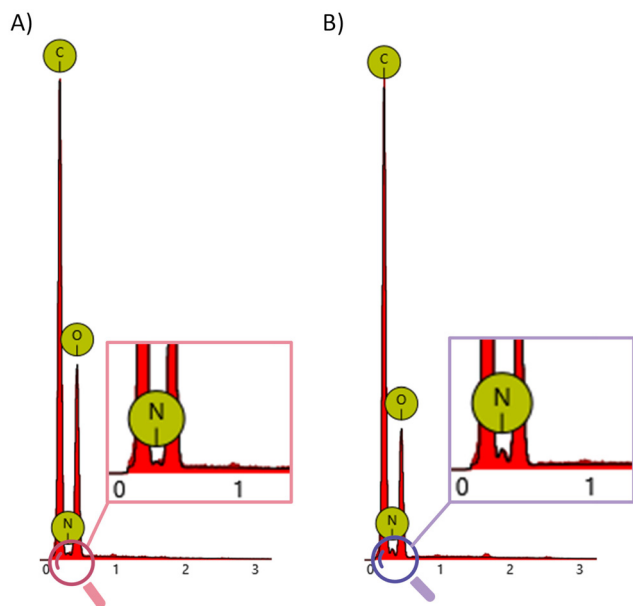
Fig. 4 EDX spectrum of (A) PEU scaffold and (B) PEU-col scaffold.

sample of defined weight (37 mg). The hydroxyproline mass present in the sample was determined to be 0.0325 ± 0.0013 mg, calculated with the linear fit of the calibration curve (see Fig. S6†). Considering that hydroxyproline constitu-

tes 13% of collagen, it corresponds to 0.262 ± 0.026 mg of collagen in the scaffold, *i.e.*, 0.7 wt%. As the two methods led to slightly different values (0.3 wt% by EDX and 0.7 wt% by hydroxyproline dosage) a final method was followed. Col-FITC coated on a scaffold was released in 10 mL of acid acetic and the fluorescence of this solution was measured. The collagen concentration was evaluated with the calibration curve of Col-FITC (see Fig. S7†).

The percentage evaluated with this method was slightly lower than the other techniques probably due to the lower commercial Col-FITC concentration (1 mg mL^{-1}) used for the forced infiltration (against 3 mg mL^{-1} for non-labelled Col-I). Results as a function of the technique are listed in Fig. 3A. The collagen values were higher than values found by Chang *et al.*[29] (349 ± 7.6 µg per scaffold, for a scaffold volume of 98 × 10^{-3} cm^3 compared with 300 µg per scaffold, for a smaller volume $V = 0.2 \times 10^{-3}$ cm^3) with a poly(ε-caprolactone) scaffold chemically grafted with a type II collagen.

After coating, the PEU-Col scaffolds were analysed by SEM (Fig. 5A) showing a pore size of 188 ± 59 µm (Fig. 5B), similar to that of pristine PEU scaffolds, suggesting a very thin layer of collagen coating. The mechanical properties of the scaffolds coated with collagen were investigated (as seen in Fig. 5C and D). The Young's modulus was 0.37 ± 0.14 MPa, the storage modulus was 6.14 MPa at 25 °C, and 1.4 MPa at 37 °C.

These values are slightly higher but in the same range as that for the pristine PEU-scaffold (E_y = 0.2 ± 0.2 MPa), which is
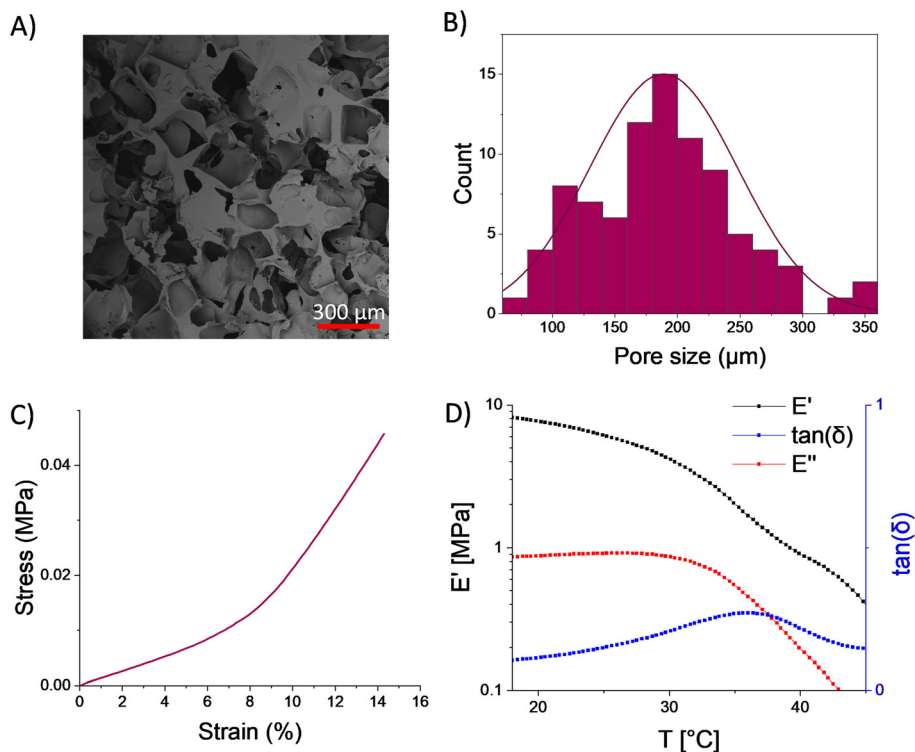

Fig. 5 Morphological and mechanical characterization of the PEU-Col scaffold. (A) SEM micrograph of the inner part of a PEU-Col scaffold, (B) pore size distribution of a PEU-Col scaffold, (C) typical stress/strain compression curve under dry conditions at RT, and (D) thermo-mechanical analyses of the PEU-Col scaffold analysed by DMA (storage modulus E', loss modulus E'' and loss factor tan(δ)).

not surprising considering the expected low contribution of 0.3 wt% collagen located only at the surface of the pores, and the low mechanical properties of collagen compared to the ones of PEU. A similar trend was also observed on the β-tricalcium phosphate scaffold double coated with collagen, with compression strength mean values at 0.022 ± 0.012 MPa, compared to the values of 0.024 ± 0.012 MPa before coating.[48]

Wagner *et al.* also worked on incorporating collagen in poly (ester urethane)urea (PEUU) to incorporate bioactivity and increase cellular interaction. The PEUU was obtained from butanediisocyanate, PCL (M_w = 2000 g mol^{-1}) and putrescine for soft tissue engineering applications. Type I acid soluble bovine collagen was incorporated (at different concentrations, ranging from 0 to 90 wt%) into the polymer film using the electrospinning technique by blending the PEUU with collagen in hexafluoro-2-propanol. Despite an important porosity of 85%, the pores size was relatively smaller (50 μm) compared to our samples, due to the electrospinning technique used. The targeted cardiac application led to mechanical evaluations with tensile tests that cannot be compared with our systems,[49,50] however, an *in vivo* study showed that these PEUU scaffolds had endocardial endothelialization at 4 weeks, with a moderate inflammatory reaction.

3.4. Morphological study of PEU-Col scaffolds

For a more in-depth study of the scaffolds, X-ray micro-computed tomography (μCT) was then used. A 3D-volumetric image was obtained by stacking successive 2D cross sections of the scaffold (see Fig. S8†). At first, the PEU scaffold and PEU-Col scaffold were compared. In Fig. 6A and D white regions correspond respectively to PEU or PEU-Col whereas black regions correspond to air. In Fig. 6B and E an overall reconstruction of the scaffolds is shown. The analysis led to the calculation of a porosity of 76 ± 3% for the PEU scaffold (comparable to the value of 76 ± 1% obtained by density functional calculations, see section 3.2) and 74 ± 2% for the PEU-Col scaffold. The slight porosity decrease is explained by the collagen coating.

Fig. 6C shows the uniform pore size range of the PEU scaffold of 100–300 μm (in green), which confirmed the results obtained by SEM. In more detail, mathematical calculation from the software indicated the presence of two populations on PEU scaffold images: one in the range of 100–333 μm (41%) and one in the range of 33–99 μm (59%) which could correspond to the connections between the pores. The pore size of PEU-Col was smaller, as shown by the blue colour in Fig. 6F and pore size distribution in Fig. 6I, as a result of the presence of the collagen layer decreasing the pore size.

Since collagen and PEU are polymers with similar density, it is not possible to distinguish them in the μCT images. To overcome this limitation, a PEU scaffold was coated with a collagen solution saturated with iohexol as a contrast agent. Fig. 6G shows a single 2D cross section where white regions correspond to the part of the matrix of PEU coated with collagen (saturated with iohexol). This additional analysis revealed some heterogeneity in the collagen repartition,

denser on the edges of the scaffold compared to the core. This difference is explained by the incorporation method with forced infiltration of the collagen solution through the bulky material. When the collagen solution penetrates the pores, air is entrapped and compressed in the middle of the sample, which results in a partial blocking of the collagen solution that flows more freely in the pores of the outer regions. This heterogeneity is however not considered as a problem to overcome, since cells in contact with the material will first encounter collagen-rich regions before further infiltrating the scaffolds and reach the collagen-depleted central region. Actually, the alveolar structuration of the PEU matrix (Fig. 6A, B, D and E) and the deposition of collagen after forced infiltration confirm the porous network interconnectivity (as illustrated in Movie 1 for the PEU scaffold, see the ESI†) that can enable cell migration.

3.5. Sterilization

Considering the mandatory sterility for implantable medical devices and scaffolds, PEU scaffolds were subjected to beta-ray irradiation to evaluate the impact on the PEU. A dose of 25 kGy was selected as it is a typical dose applied to medical devices.[51,52] Depending on the polymer nature the two-concomitant process of chain scission and crosslinking can occur to different extents under such sterilization conditions.[53] Typically, the crosslinking can be highlighted by an increase in the weight average molecular weight and in the dispersity. In fact, as seen on the chromatogram showing the diffraction index and Rayleigh responses (see Fig. 7A), two populations can be deduced from the Rayleigh response. The weight average molecular weight increased from M_w = 35 000 kg mol^{-1} ($Đ$ = 2.4) before sterilization to M_w = 37 000 kg mol^{-1} ($Đ$ = 4.1) after sterilization.

Mechanical analyses were performed on the PEU-scaffold after sterilization, as seen in Fig. 7B, showing no decrease of the Young's modulus before and after sterilization (E_y PEU scaffold sterilized = 0.20 ± 0.02 MPa *vs.* E_y PEU scaffold = 0.23 ± 0.02 MPa).

3.6. Cell studies

In order to assess the biocompatibility of the PEU scaffolds, a cytotoxicity study was first carried out using a CellTiter-Glo® assay. The scaffolds were compared to TCPS as well as two control samples, positive RM-A and negative RM-C, in accordance with the European standard NF EN ISO 10993. As shown in Fig. 8A, the percentage of viable L929 murine fibroblasts upon contact with the PEU scaffolds was 75% against 81% for the negative RM-C control, and surpassing the 70% threshold set by the European standard (indicated by the orange dotted lines). This outcome confirms the absence of acute cytotoxicity of the scaffolds and validates the various process steps used for the preparation of the pristine PEU scaffolds.

The proliferation of L929 murine fibroblasts was then assessed with the different scaffolds to evaluate the impact of the collagen incorporation. With the exception of the first time point at 2 days, where similar proliferations were found on all
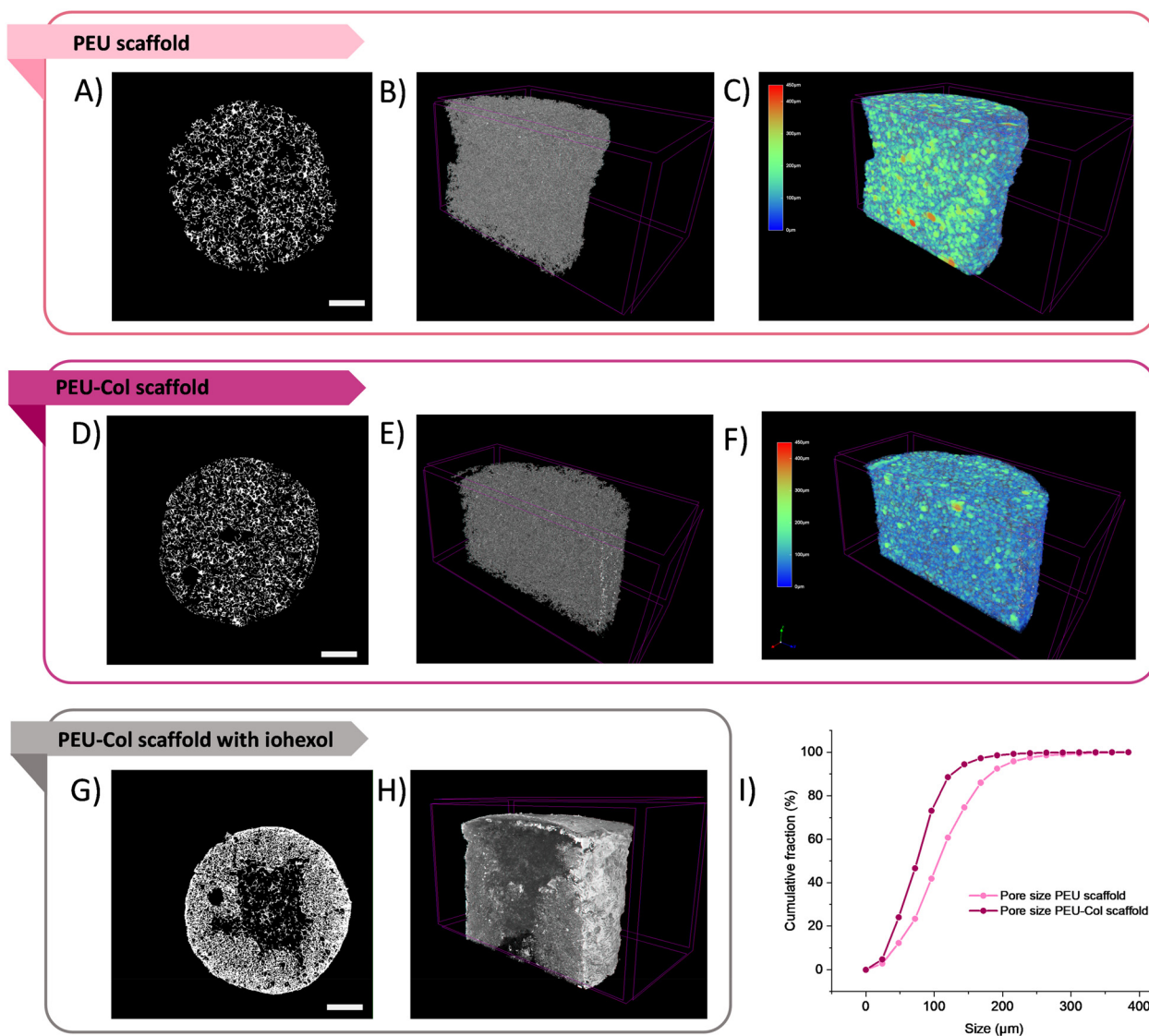
Fig. 6 Morphological studies of the scaffolds by micro-computed tomography. Representative µCT images of scaffolds: single 2D slices of (A, D and G) PEU, PEU-Col and PEU-Col iohexol scaffolds, respectively. White regions correspond to PEU (A) or PEU-Col (D) matrix or to the part of the PEU matrix coated with collagen (G). Global µCT image of (B, E and H) PEU, PEU-Col, and PEU-Col with iohexol scaffolds, respectively, and (C and F) with color scale corresponding to the pore size. (I) Cumulative fraction of pore size of PEU and PEU-Col scaffolds.

scaffolds, the PEU-Col scaffold always led to higher proliferation (Fig. 8B). After 9 days, proliferation was already significantly improved (127% with respect to TCPS) compared to the commercial Actifit® implant (56%). After 14 days, the trend was even more pronounced with PEU-Col scaffolds exhibiting much higher cell proliferation (114% with respect to TCPS) compared to the PEU scaffold (58%) and largely outperforming the commercial gold standard Actifit® (38%), as illustrated in Fig. S9.† It is remarkable that proliferation was even better than on the TCPS control and this result is highly encouraging to envision future development with other cells like chondrocytes. For example, PCL-diol/HDI based PEU grafted with collagen showed lower proliferation of chondrogenic cells compared to TCPS.[54] In another study, poly(ester-carbonate-urea-

urethane) obtained from oligo(tetramethylene succinate-*co*-carbonate) diols and HDI were coated with collagen by simple incubation and the resulting material, despite being non-cytotoxic, showed about twice lower human keratinocyte cell proliferation compared to the TCPS control.[55]

The morphology of cells was also observed by fluorescence microscopy (Fig. 8C–E). Assuming that the cells are uniformly distributed, it is inferred from the pictures that the scaffolds possess appropriate pore size and porosity, facilitating cell infiltration. However, a denser layer of cells can be observed on the PEU-Col scaffold, which is in line with the higher percentage of proliferation for this scaffold compared to the others. Additionally, the characteristic spindle-shaped form of the cells observed on the surface of PEU-Col scaffolds suggests
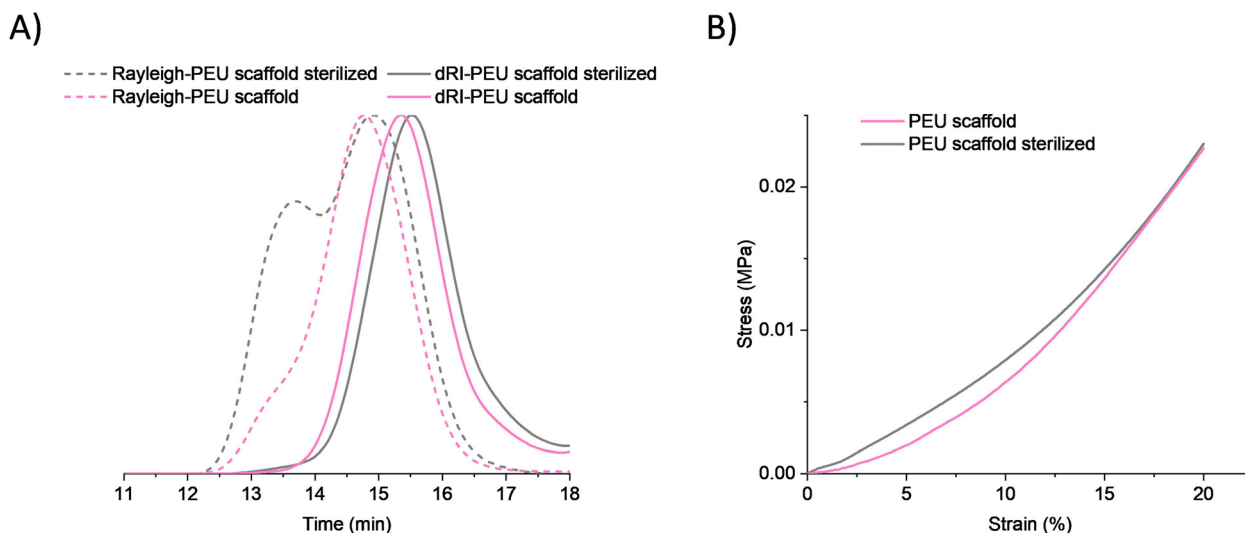
A)

B)

Fig. 7 Impact of the sterilization on the PEU scaffolds. Characterization of the PEU-scaffold before and after beta sterilization by (A) SEC-MALS analysis and the (B) typical stress/strain compression curve of PEU scaffold after beta sterilization.

a higher affinity of cells towards these scaffolds, as seen in Fig. S10.† In contrast, the cells on the PEU scaffold and on the gold standard Actifit® exhibit a round-shaped form, indicating a lower affinity of the cells with the materials. This set of results confirms that the collagen coated in the PEU-Col scaffold not only enhances cell proliferation but also offers a better cell/surface affinity to improve tissue regeneration. This phenomenon was also observed by Bahcecioglu *et al.* where fibrochondrocytes elongated and aligned along the collagen fibres.[56] They also showed that cell behaviour was correlated with the pore size and strut mechanical properties of the scaffold. In our study, the gold standard, PEU and PEU-Col scaffolds exhibit similar mechanical properties and pore size, we could suggest that the presence of collagen could enhance the biological properties of the scaffold.

3.7. Degradation

To evaluate the degradation profile of the scaffolds, specimens were subjected to *in vitro* degradation in PBS at pH 7.4. The pH of the solution decreased faster for the PEU scaffolds compared to the commercial gold standard and the medium was refreshed when pH decreased by 5%, as illustrated in Fig. S11.† This is due to the faster degradation induced by the presence of PLGA segments degraded in lactic and glycolic acid that are not present in the PCL-based Actifit® implant. Fig. 9A shows the evolution of the residual mass of the scaffolds over a 6 month period. After 12 months, the mass of the gold standard remains unchanged, whereas PEU scaffolds already witness a 40% mass loss after 2 months. It was not possible to follow up the degradation after 2 months, due to the samples falling into pieces when rinsing with distilled water, as seen in the picture in Fig. 9A. These results are consistent with the slow degradation of PCL (from 2 to 8 years *in vitro*[57]) that is the only component of the Actifit® gold stan-

dard, compared to the faster degradation of PLGA segments. This slow degradation can lead to loss of connection between the scaffold and the surrounding tissue, and thus delay the healing process.[58,59]

Changes in the Young's modulus of the scaffolds during *in vitro* degradation are shown in Fig. 9B. We can observe a fast decrease of the Young's modulus of PEU scaffolds with a $E_y = 0.05 \pm 0.02$ MPa, after 28 days of degradation, compared to $E_y = 0.27 \pm 0.09$ MPa. This rapid loss of properties is not necessarily detrimental and should be put in perspective with the much-improved cellular proliferation and cell affinity towards PEU-Col scaffolds, which may turn to a faster meniscus regeneration and recovery of the mechanical properties *via* the formation of a neo-tissue.

Regarding the evolution of molecular weight over time (see Fig. 9C for the evolution of light scattering signals over time), the PEU scaffolds experienced an 80% reduction in molar mass within a period of 15 days. In contrast, it took around 28 days to achieve the same level of reduction for the PCL-based gold standard (Fig. 9D). This difference is most likely attributed to the differential degradation of the PLGA blocks within our PEU scaffold, which tends to break down more rapidly into smaller water-soluble oligomers capable of diffusing out of the matrix. This phenomenon elucidates the swift decline in mass. Conversely, the gold standard scaffold is composed of PCL segments that degrade at a slower rate and yield hydrophobic oligomers which, at similar polymerization degrees, exhibit lower solubility compared to their PLGA counterparts. Consequently, these oligomers are less inclined to diffuse out of the scaffold. Regarding the dispersity measured by SEC for the PEU scaffolds, it remained stable ($Đ = 1.5$) for 60 days. In contrast, the dispersity of gold standard dropped from $Đ = 3.04$ to 1.6, which underlines the elimination of fragments of the second population on the chromatogram (as seen in Fig. S12†).
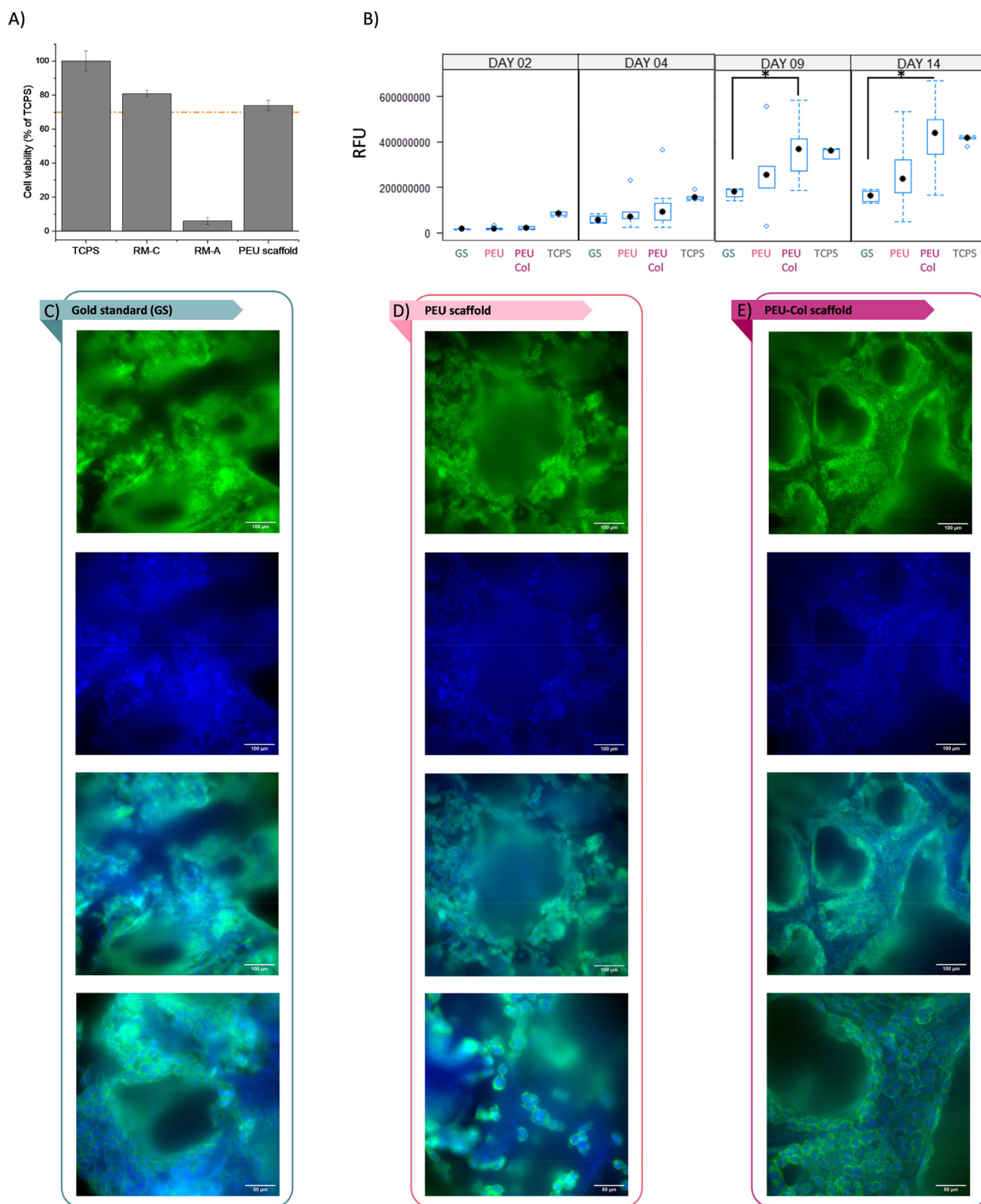
Fig. 8 Evaluation of scaffolds cytotoxicity and cell proliferation. (A) L929 cells viability with PEU scaffolds evaluated by the extract method (24 hours, NF EN ISO 10993). Data are expressed as means ± SD and correspond to measurements with $n = 3$. (B) Boxplot of L929 proliferation on the different scaffolds after 2, 4, 9 and 14 days. The fibroblasts were seeded on TCPS ($n = 6$), Actifit® gold standard ($n = 4$), PEU scaffold ($n = 6$) and PEU-Col scaffold ($n = 6$), and cultured for 14 days. (C–E) L929 fibroblasts morphology observed under a Leica Thunder microscope for (C) Actifit® gold standard, (D) PEU scaffold and (E) PEU-Col scaffold. L929 fibroblasts morphology was observed using phalloidin iFluor 488 (F-actin stained in green, first line of images) and Hoechst (nucleus in blue, second line of images). The third and fourth images illustrate the merged images with scale bar corresponding to 100 μm, and 50 μm, respectively. * Indicates a significant difference between groups (*$p < 0.05$).
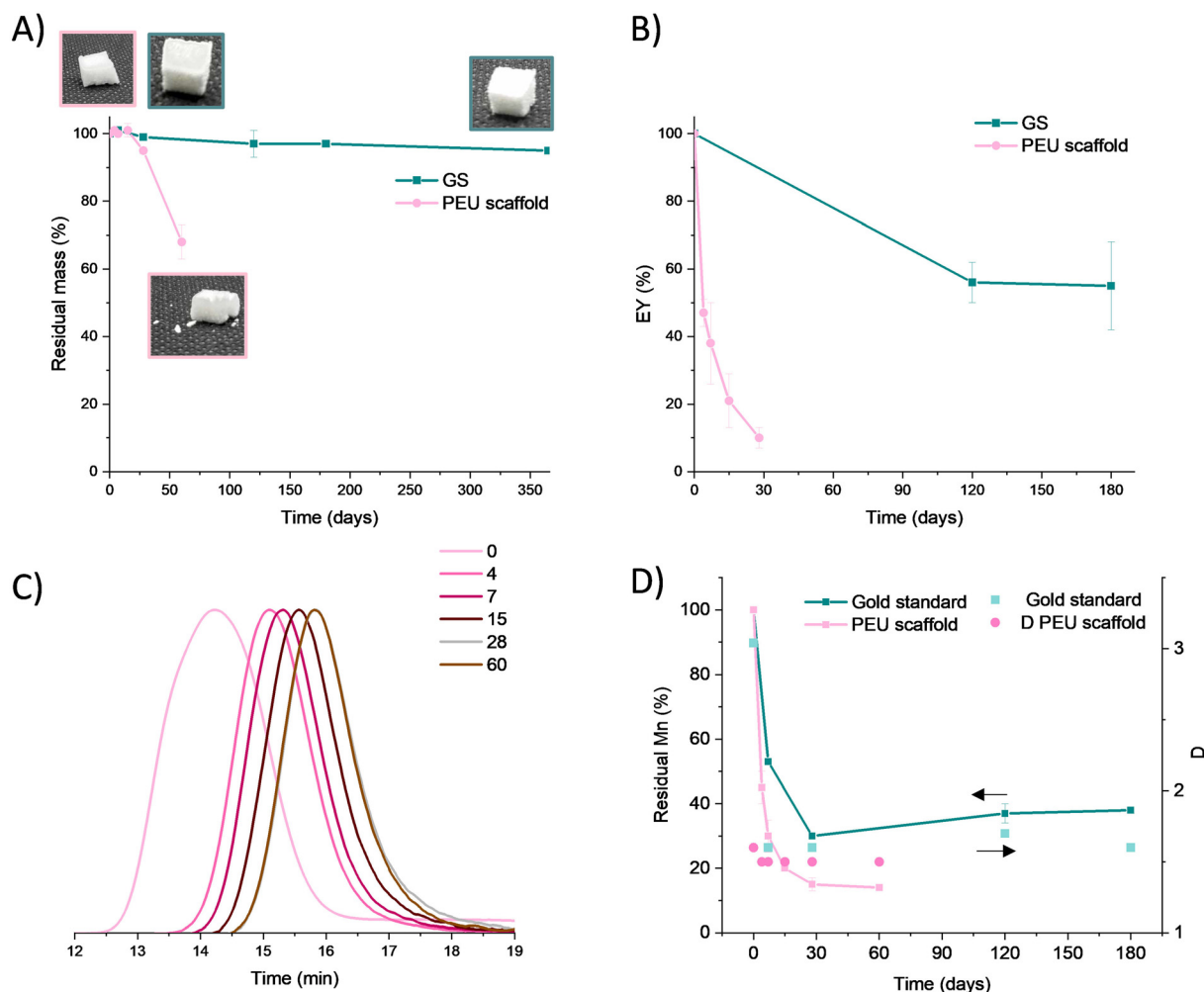
Fig. 9 Comparison of the *in vitro* degradation (PBS, 37 °C, pH = 7.4) of the gold standard scaffold and PEU scaffold. (A) Evolution of residual mass over time with pictures of the scaffold at day 0, day 60 for PEU scaffolds, and day 120 for Actifit® gold standard, (B) evolution of Young's modulus E_y over time, (C) evolution of light scattering (SEC-MALS, THF) signals of PEU scaffold samples over time (the numbers in the legend corresponds to days). (D) Evolution of residual molecular weight and dispersity over time. Data are expressed as means $\pm$ SD and correspond to measurement with n = 3.

4. Conclusions

A polyester-polyurethane (PEU) polymer with a M_n of 52~ kg mol^{-1} was synthesized in a two-step process using a PCL pre-polymer functionalized with LDI, and PLGA-diol as a chain extender. This polymer was turned into a 3D porous scaffold with a defined pore size and mechanical properties using an SC/PL process with sodium chloride as the porogen agent. SEM and tomography reconstruction confirmed that the scaffold had a relatively uniform pore size of around 170 μm and an overall porosity of 74%, corresponding to open porosity. The deposition of collagen through forced infiltration is a consequence of the interconnection of the porous network that is essential for cell proliferation. The mechanical properties were evaluated and close to the human meniscus. To enhance the biological properties, different techniques were investigated to physically bond collagen type I: immersion, injection and forced infiltration. The latest method was proved

to be the more efficient to build a hybrid scaffold with collagen. Different techniques such as SEM-EDX, hydroxyproline titration and Col-FITC titration showed that 0.3 wt% of Col-I were incorporated into the scaffold. Cytotoxicity studies revealed the biocompatibility of the PEU scaffold of 75% viability of L929 cells. The proliferation study showed that the collagen coating not only influences cell proliferation, but also provides a better cell affinity with the material. A degradation study in PBS revealed that PLGA blocks in the PEU scaffold could greatly influence the degradation rate, compared to the gold standard: Young's modulus and molecular mass decreased by 80% after 30 days of incubation. Despite a fast degradation rate, the composition of this PEU scaffold could allow fast cell proliferation and limit the presence of residual fragments that could elicit a body response. This study confirms the potential of these scaffolds as meniscal replacement and articular cartilage repair and opens the way to other investigations. Supplementary *in vitro* assays will be performed

with cells in accordance with the application (*i.e.*, chondrocytes) and *in vivo* assays will also be investigated.

Author contributions

Gaëlle Savin: data curation, formal analysis, investigation, methodology, resources, writing – original draft, and writing – review & editing. Sylvain Caillol: conceptualization, funding acquisition, resources, supervision, validation, and writing – review & editing. Audrey Bethry: formal analysis, investigation, and writing – review & editing. Eric Rondet: data curation, formal analysis, investigation, and writing – review & editing. Michel Assor: conceptualization and funding acquisition. Ghislain David: conceptualization, funding acquisition, project administration, resources, supervision, validation, and writing – review & editing. Benjamin Nottelet: conceptualization, funding acquisition, project administration, resources, supervision, validation, and writing – review & editing.

Conflicts of interest

Gaëlle Savin and MD. Michel Assor are employees of Arthrocart Biotech. All other authors declare no conflicts of interest.

Acknowledgements

References

1 A. I. Bochynska, *Development of biodegradable adhesives for meniscus repair*, University of Twente, 2016. DOI: **10.3990/1.9789036541527**.

2 T. G. Tienen, R. G. J. C. Heijkants, P. Buma, J. H. De Groot, A. J. Pennings and R. P. H. Veth, A porous polymer scaffold for meniscal lesion repair - A study in dogs, *Biomaterials*, 2003, **24**, 2541–2548, DOI: **10.1016/S0142-9612(03)00053-X**.

3 P. Buma, T. van Tienen and R. P. Veth, The collagen meniscus implant, *Expert Rev. Med. Devices*, 2007, **4**, 507–516, DOI: **10.1586/17434440.4.4.507**.

4 H. Vignes, G. Conzatti, G. Hua and N. Benkirane-Jessel, Meniscus Repair: From In Vitro Research to Patients, *Organoids*, 2022, **1**, 116–134, DOI: **10.3390/organoids1020010**.

5 E. Bulgheroni, A. Grassi, M. Campagnolo, P. Bulgheroni, A. Mudhigere and A. Gobbi, Comparative Study of Collagen versus Synthetic-Based Meniscal Scaffolds in Treating Meniscal Deficiency in Young Active Population, *Cartilage*, 2016, **7**, 29–38, DOI: **10.1177/1947603515600219**.

6 V. Martinek, P. Ueblacker, K. Bräun, S. Nitschke, R. Mannhardt, K. Specht, B. Gansbacher and A. B. Imhoff, Second generation of meniscus transplantation: in vivo study with tissue engineered meniscus replacement, *Arch. Orthop. Trauma Surg.*, 2006, **126**, 228–234, DOI: **10.1007/s00402-005-0025-1**.

7 J. de Groot, Actifit, Polyurethane meniscus implant: basic science, in *The Meniscus*, Springer Berlin Heidelberg, Berlin, Heidelberg, 2010, pp. 383–387. DOI: **10.1007/978-3-642-02450-4_48**.

8 H. Zhang, L. Zhou and W. Zhang, Control of scaffold degradation in tissue engineering: A review, *Tissue Eng., Part B*, 2014, **20**, 492–502, DOI: **10.1089/ten.teb.2013.0452**.

9 J. Kucinska-Lipka, M. Marzec, I. Gubanska and H. Janik, Porosity and swelling properties of novel polyurethane-ascorbic acid scaffolds prepared by different procedures for potential use in bone tissue engineering, *J. Elastomers Plast.*, 2017, **49**, 440–456, DOI: **10.1177/0095244316672093**.

10 N. Thadavirul, P. Pavasant and P. Supaphol, Development of polycaprolactone porous scaffolds by combining solvent casting, particulate leaching, and polymer leaching techniques for bone tissue engineering, *J. Biomed. Mater. Res., Part A*, 2014, **102**, 3379–3392, DOI: **10.1002/jbm.a.35010**.

11 H. Janik and M. Marzec, A review: Fabrication of porous polyurethane scaffolds, *Mater. Sci. Eng., C*, 2015, **48**, 586–591, DOI: **10.1016/j.msec.2014.12.037**.

12 L. Cen, W. Liu, L. Cui, W. Zhang and Y. Cao, Collagen Tissue Engineering: Development of Novel Biomaterials and Applications, *Pediatr. Res.*, 2008, **63**, 492–496, DOI: **10.1203/pdr.0b013e31816c5bc3**.

13 Z. Li, N. Wu, J. Cheng, M. Sun, P. Yang, F. Zhao, J. Zhang, X. Duan, X. Fu, J. Zhang, X. Hu, H. Chen and Y. Ao, Biomechanically, structurally and functionally meticulously tailored polycaprolactone/silk fibroin scaffold for meniscus regeneration, *Theranostics*, 2020, **10**, 5090, DOI: **10.7150/THNO.44270**.

14 M. A. Salati, J. Khazai, A. M. Tahmuri, A. Samadi, A. Taghizadeh, M. Taghizadeh, P. Zarrintaj, J. D. Ramsey, S. Habibzadeh, F. Seidi, M. R. Saeb and M. Mozafari, Agarose-Based Biomaterials: Opportunities and Challenges in Cartilage Tissue Engineering, *Polymers*, 2020, **12**, 1150, DOI: **10.3390/POLYM12051150**.

15 T. Murakami, S. Otsuki, Y. Okamoto, K. Nakagawa, H. Wakama, N. Okuno and M. Neo, Hyaluronic acid promotes proliferation and migration of human meniscus cells via a CD44-dependent mechanism, *Connect. Tissue Res.*, 2019, **60**, 117–127, DOI: **10.1080/03008207.2018.1465053**.

16 R. Resmi, J. Parvathy, A. John and R. Joseph, Injectable self-crosslinking hydrogels for meniscal repair: A study with oxidized alginate and gelatin, *Carbohydr. Polym.*, 2020, **234**, 115902, DOI: **10.1016/J.CARBPOL.2020.115902**.

17 E. A. Makris, P. Hadidi and K. A. Athanasiou, The knee meniscus: structure-function, pathophysiology, current repair techniques, and prospects for regeneration, *Biomaterials*, 2011, **32**, 7411–7431, DOI: **10.1016/J. BIOMATERIALS.2011.06.037**.

18 R. Al Nakib, A. Toncheva, V. Fontaine, J. Vanheuverzwijn, J. Raquez and F. Meyer, Thermoplastic polyurethanes for biomedical application: A synthetic, mechanical, antibacterial, and cytotoxic study, *J. Appl. Polym. Sci.*, 2022, **139**, 51666, DOI: **10.1002/app.51666**.

19 D. K. Dempsey, J. L. Robinson, A. V. Iyer, J. P. Parakka, R. S. Bezwada and E. M. Cosgriff-Hernandez, Characterization of a resorbable poly(ester urethane) with biodegradable hard segments, *J. Biomater. Sci., Polym. Ed.*, 2014, **25**, 535–554, DOI: **10.1080/09205063.2014.880247**.

20 B. Naureen, A. S. M. A. Haseeb, W. J. Basirun and F. Muhamad, Recent advances in tissue engineering scaffolds based on polyurethane and modified polyurethane, *Mater. Sci. Eng., C*, 2021, **118**, 111228, DOI: **10.1016/j.msec.2020.111228**.

21 K. Gorna and S. Gogolewski, Biodegradable porous polyurethane scaffolds for tissue repair and regeneration, *J. Biomed. Mater. Res., Part A*, 2006, **79**, 128–138, DOI: **10.1002/jbm.a.30708**.

22 Y. Gong, Y. Zhu, Y. Liu, Z. Ma, C. Gao and J. Shen, Layer-by-layer assembly of chondroitin sulfate and collagen on aminolyzed poly(l-lactic acid) porous scaffolds to enhance their chondrogenesis, *Acta Biomater.*, 2007, **3**, 677–685, DOI: **10.1016/j.actbio.2007.04.007**.

23 M. Zuber, F. Zia, K. M. Zia, S. Tabasum, M. Salman and N. Sultan, Collagen based polyurethanes-A review of recent advances and perspective, *Int. J. Biol. Macromol.*, 2015, **80**, 366–374, DOI: **10.1016/j.ijbiomac.2015.07.001**.

24 R. Parenteau-Bareil, R. Gauvin and F. Berthod, Collagen-Based Biomaterials for Tissue Engineering Applications, *Materials*, 2010, **3**, 1863–1887, DOI: **10.3390/ma3031863**.

25 A. M. Ferreira, P. Gentile, V. Chiono and G. Ciardelli, Collagen for bone tissue regeneration, *Acta Biomater.*, 2012, **8**, 3191–3200, DOI: **10.1016/j.actbio.2012.06.014**.

26 S. Nehrer, Chondrocyte-seeded collagen matrices implanted in a chondral defect in a canine model, *Biomaterials*, 1998, **19**, 2313–2328, DOI: **10.1016/S0142-9612(98)00143-4**.

27 Z. Ma, C. Gao, J. Ji and J. Shen, Protein immobilization on the surface of poly-L-lactic acid films for improvement of cellular interactions, *Eur. Polym. J.*, 2002, **38**, 2279–2284, DOI: **10.1016/S0014-3057(02)00119-2**.

28 Z. Ma, C. Gao, Y. Gong, J. Ji and J. Shen, Immobilization of natural macromolecules on poly-L-lactic acid membrane surface in order to improve its cytocompatibility, *J. Biomed. Mater. Res.*, 2002, **63**, 838–847, DOI: **10.1002/jbm.10470**.

29 K. Y. Chang, L. H. Hung, I. M. Chu, C. S. Ko and Y. Der Lee, The application of type II collagen and chondroitin sulfate grafted PCL porous scaffold in cartilage tissue engineering, *J. Biomed. Mater. Res., Part A*, 2010, **92**, 712–723, DOI: **10.1002/jbm.a.32198**.

30 M. Lelli, I. Foltran, E. Foresti, J. Martinez-Fernandez, C. Torres-Raya, F. M. Varela-Feria and N. Roveri, Biomorphic silicon carbide coated with an electrodeposition of nanostructured hydroxyapatite/collagen as biomimetic bone filler and scaffold, *Adv. Eng. Mater.*, 2010, **12**, 348–355, DOI: **10.1002/adem.200980086**.

31 S. Potorac, M. Popa, V. Maier, G. Lisa and L. Verestiuc, New hydrogels based on maleilated collagen with potential applications in tissue engineering, *Mater. Sci. Eng., C*, 2012, **32**, 236–243, DOI: **10.1016/j.msec.2011.10.024**.

32 J. Guan, J. J. Stankus and W. R. Wagner, Development of composite porous scaffolds based on collagen and biodegradable poly(ester urethane)urea, *Cell Transplant.*, 2006, **15**, 17–27, DOI: **10.3727/000000006783982412**.

33 J. Hum and A. Boccaccini, Collagen as Coating Material for 45S5 Bioactive Glass-Based Scaffolds for Bone Tissue Engineering, *Int. J. Mol. Sci.*, 2018, **19**, 1807, DOI: **10.3390/ijms19061807**.

34 Y. S. Pek, S. Gao, M. S. M. Arshad, K. J. Leck and J. Y. Ying, Porous collagen-apatite nanocomposite foams as bone regeneration scaffolds, *Biomaterials*, 2008, **29**, 4300–4305, DOI: **10.1016/j.biomaterials.2008.07.030**.

35 K. Von der Mark, Structure, Biosynthesis and Gene Regulation of Collagens in Cartilage and Bone, in *Dynamics of Bone and Cartilage Metabolism*, Elsevier, 2006, pp. 3–40. DOI: **10.1016/B978-012088562-6/50002-9**.

36 Y. H. Li and Y. D. Huang, The study of collagen immobilization on polyurethane by oxygen plasma treatment to enhance cell adhesion and growth, *Surf. Coat. Technol.*, 2007, **201**, 5124–5127, DOI: **10.1016/j.surfcoat.2006.07.128**.

37 R. Chen, C. Huang, Q. Ke, C. He, H. Wang and X. Mo, Preparation and characterization of coaxial electrospun thermoplastic polyurethane/collagen compound nanofibers for tissue engineering applications, *Colloids Surf., B*, 2010, **79**, 315–325, DOI: **10.1016/j.colsurfb.2010.03.043**.

38 G. Savin, O. Sastourne-Array, S. Caillol, A. Bethry, M. Assor, G. David and B. Nottelet, Evaluation of Porous (Poly (lactide-co-glycolide)-co-(ε-caprolactone)) Polyurethane for Use in Orthopedic Scaffolds, *Molecules*, 2024, **29**, 766, DOI: **10.3390/molecules29040766**.

39 J. F. Woessner, The determination of hydroxyproline in tissue and protein samples containing small proportions of this imino acid, *Arch. Biochem. Biophys.*, 1961, **93**, 440–447, DOI: **10.1016/0003-9861(61)90291-0**.

40 L. A. Feldkamp, L. C. Davis and J. W. Kress, *Practical cone-beam algorithm*, 1984.

41 G. Yan, J. Tian, S. Zhu, Y. Dai and C. Qin, *Fast cone-beam CT image reconstruction using GPU hardware*, IOS Press, 2008. **https://www.researchgate.net/publication/228624487**.

42 W. E. Lorensen and H. E. Cline, *Marching cubes: A high resolution 3D surface construction algorithm*, 1987. DOI: **10.1145/37402.37422**.

43 G. Borgefors, On Digital Distance Transforms in Three Dimensions, in *Computer Vision and Image Understanding*, 1996, vol. 64, pp. 368–376. DOI: **10.1006/cviu.1996.0065**.

44 E. Remy and E. Thiel, Medial axis for chamfer distances: computing look-up tables and neighbourhoods in 2D or 3D, *Pattern Recognit. Lett.*, 2002, **23**, 649–661, DOI: **10.1016/S0167-8655(01)00141-6**.

45 P. Bruin, G. J. Veenstra, A. J. Nijenhuis and A. J. Pennings, Design and synthesis of biodegradable poly(ester-urethane) elastomer networks composed of non-toxic building blocks, *Makromol. Chem., Rapid Commun.*, 1988, **9**, 589–594, DOI: **10.1002/marc.1988.030090814**.

46 B. Saad, T. D. Hirt, M. Welti, G. K. Uhlschmid, P. Neuenschwander and U. W. Suter, *Development of degradable polyesterurethanes for medical applications: In vitro and in vivo evaluations*, 1997.

47 M. A. Sweigart, C. F. Zhu, D. M. Burt, P. D. Deholl, C. M. Agrawal, T. O. Clanton and K. A. Athanasiou, *Intraspecies and Interspecies Comparison of the Compressive Properties of the Medial Meniscus*, 2004.

48 A. Sharma, N. Aggarwal, S. Rastogi, R. Choudhury and S. Tripathi, Effectiveness of platelet-rich fibrin in the management of pain and delayed wound healing associated with established alveolar osteitis (dry socket), *Eur. J. Dent.*, 2017, **11**, 508–513, DOI: **10.4103/ejd.ejd_346_16**.

49 K. L. Fujimoto, J. Guan, H. Oshima, T. Sakai and W. R. Wagner, In Vivo Evaluation of a Porous, Elastic, Biodegradable Patch for Reconstructive Cardiac Procedures, *Ann. Thorac. Surg.*, 2007, **83**, 648–654, DOI: **10.1016/j.athoracsur.2006.06.085**.

50 J. J. Stankus, J. Guan and W. R. Wagner, Fabrication of biodegradable elastomeric scaffolds with sub-micron morphologies, *J. Biomed. Mater. Res., Part A*, 2004, **70**, 603–614, DOI: **10.1002/jbm.a.30122**.

51 H. Nguyen, D. A. F. Morgan and M. R. Forwood, Sterilization of allograft bone: Is 25 kGy the gold standard for gamma irradiation?, *Cell Tissue Banking*, 2007, **8**, 81–91, DOI: **10.1007/s10561-006-9019-7**.

52 V. Hasirci, F. Berthiaume, S. P. Bondre, J. D. Gresser, D. J. Trantolo, M. Toner and D. L. Wise, Expression of Liver-Specific Functions by Rat Hepatocytes Seeded in Treated Poly(Lactic- co -Glycolic) Acid Biodegradable Foams, *Tissue Eng.*, 2001, **7**, 385–394, DOI: **10.1089/10763270152436445**.

53 M. Gradwohl, F. Chai, J. Payen, P. Guerreschi, P. Marchetti and N. Blanchemain, Effects of two melt extrusion based additive manufacturing technologies and common sterilization methods on the properties of a medical grade PLGA copolymer, *Polymers*, 2021, **13**, 1–15, DOI: **10.3390/polym13040572**.

54 X. He, Z. Zhai, Y. Wang, G. Wu, Z. Zheng, Q. Wang and Y. Liu, New method for coupling collagen on biodegradable polyurethane for biomedical application, *J. Appl. Polym. Sci.*, 2012, **126**, E354–E361, DOI: **10.1002/app.36742**.

55 J. Mystkowska, M. Mazurek-Budzyńska, E. Piktel, K. Niemirowicz, W. Karalus, P. Deptuła, K. Pogoda, D. Łysik, J. R. Dąbrowski, G. Rokicki and R. Bucki, Assessment of aliphatic poly(ester-carbonate-urea-urethane)s potential as materials for biomedical application, *J. Polym. Res.*, 2017, **24**, 144, DOI: **10.1007/s10965-017-1296-2**.

56 G. Bahcecioglu, N. Hasirci and V. Hasirci, Effects of microarchitecture and mechanical properties of 3D microporous PLLA-PLGA scaffolds on fibrochondrocyte and L929 fibroblast behavior, *Biomed. Mater.*, 2018, **13**, 035005, DOI: **10.1088/1748-605X/aaa77f**.

57 Y. Ikada and H. Tsuji, *Biodegradable polyesters for medical and ecological applications*, 2000.

58 L. Yildirimer and A. M. Seifalian, Three-dimensional biomaterial degradation - Material choice, design and extrinsic factor considerations, *Biotechnol. Adv.*, 2014, **32**, 984–999, DOI: **10.1016/j.biotechadv.2014.04.014**.

59 E. Malikmammadov, T. E. Tanir, A. Kiziltay, V. Hasirci and N. Hasirci, PCL and PCL-based materials in biomedical applications, *J. Biomater. Sci., Polym. Ed.*, 2018, **29**, 863–893, DOI: **10.1080/09205063.2017.1394711**.